Spectrum of heavy quarkonium hybrids: hyperfine splitting

Author: Sandra Tomàs Valls
*Facultat de Física, Universitat de Barcelona, Diagonal 645, 08028 Barcelona, Spain.**

Advisor: Joan Soto Riera

Abstract: Hyperfine structure of heavy quarkonium hybrids is ruled by two potentials which behaviours is only known at short and long distances. In this paper, these potentials are realistically interpolated and fitted with existing theoretical data for charmonium hybrids. Then, the spectrum of charmonium and bottomonium hybrids is calculated with a preexisting program and the hyperfine splittings are found.

I. INTRODUCTION

Some charmonium and bottomonium resonances that do not fit into the quark model spectrum have been discovered. These are called XYZ states. This identification of some exotic hadrons, tetraquark and pentaquark, that were always thought to be only a theoretical possibility has been fulfilled due to the large masses of charm and bottom quarks ($m_c, m_b \gg \Lambda_{QCD}$). Their huge masses are responsible for their slow movement and, in consequence, they see an instantaneous potential as the effective interaction. Most of the study is centered around heavy charmonium and bottomonium hybrids ($c\bar{c}$ and $b\bar{b}$ states with a non-trivial gluon content).

The work will primarily focus in the hyperfine splitting of the spectrum in hybrid quarkonium.

A. Quarkonium and hybrids

Quarkonium is a flavourless meson formed by a heavy quark and an its corresponding antiquark. However, when a field with a non-trivial gluon content is bonding the quarks, they are called hybrids. To describe their motion and energy levels, we use a non-relativistc approach due to their large masses. Moreover, making use of the Born-Oppenheimer approximation, quarkonium states can be described with the Schrödinger equation matching a stationary potential to each state of the gluon field (the gluon interaction is approximated to an instantaneous one).

To be able to calculate the hybrid spectrum it is necessary to know the hybrid potentials. Fig. 1 shows the quarkonium (Σ_g^+) and the rest of the hybrid potentials. Being only interested in the lower lying states for each potential, at leading order, we can neglect the interaction with other hybrid states with an energy $\gtrsim \Lambda_{QCD}$ above or below the low lying state. We are only going to consider the Σ_u^- and Π_u hybrid interactions and, of course, Σ_g^+.

*Electronic address: s.tomasvalls@gmail.com

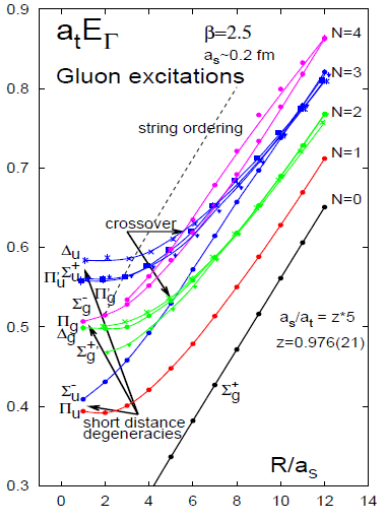

FIG. 1: Energy spectrum in the static limit for $n_f = 0$. Source: [5]

The Lagrangian chosen is [2]:

$$\mathcal{L} = tr\left(H^{i\dagger}\left(\delta_{ij} i\partial_0 - h_{Hij}\right) H_j\right) \tag{1}$$

$$h_{Hij} = \left(-\frac{\nabla^2}{m_Q} + V_{\Sigma_u^-}(r)\right)\delta_{ij} + \left(\delta_{ij} - \hat{r}_i\hat{r}_j\right)\left[V_{\Pi_u}(r) - V_{\Sigma_u^-}(r)\right]$$

We label the states with the combination of:

- NL_J: Spin multiplets. Were N is the principal quantum number; L the quark-antiquark orbital angular momentum; and J is the total angular momentum of the gluons $L_g = 1$ plus L.
- $\mathcal{J}^{PC}$: In each multiplet, the different states are $\mathcal{J}^{PC}$. $\mathcal{J}$ is the total angular momentum of the system ($\mathcal{J} = J + S$) and its third component is $\mathcal{M}$; S is the quark-antiquark spin; $P = (-1)^{L+1}$ and $C = (-1)^{L+S+1}$ are the parity and the charge conjugation (strong coupling symmetries).

In heavy quarkonium, at leading order, the spin effect could be neglected as well as in hydrogen-like atoms. But, in the next subsection, hyperfine splitting, we will take it into account as its effect is the main focus of this research. Also, we will not consider the mixing between hybrid states and quarkonium.

B. Hyperfine structure

Including the spin of the quarks into the states breaks the degeneration of each multiplet. Hyperfine splittings appear at $\mathcal{O}(1/m_Q)$ in hybrids rather than at $\mathcal{O}(1/m_Q^2)$ as in quarkonium. At leading order, they are controlled by two terms in the Lagrangian due to the P, C and T symmetries [6]:

$$\begin{aligned}\mathcal{L}_{hf} =& i\epsilon^{ijk}V_{hf}(r)tr\left(H^{i\dagger}\left[\sigma^k,H^j\right]\right)+\\ &+ir^i\epsilon^{ijk}V_{hf2}(r)tr\left(r^iH^{i\dagger}\left[\sigma^k,H^j\right]\right)+H.c.\end{aligned} \tag{2}$$

There are two potentials and their form allows us to separate a global factor $-2V_{hf}(r)$ and $-2V_{hf2}(r)$ from its corresponding Hamiltonian H_{hf} and H_{hf2}. In the $|(S=1)LJ\mathcal{J}\mathcal{M}\rangle$ basis:

For $J>1$ we can separate the 9x9 matrix intro two boxes. The five dimensional box corresponds to the subspace spanned by $((P^{--}_{1\mathcal{J}\mathcal{M}},P^{+-}_{1\mathcal{J}\mathcal{M}},P^{00}_{1\mathcal{J}\mathcal{M}},P^{-+}_{1\mathcal{J}\mathcal{M}},P^{++}_{1\mathcal{J}\mathcal{M}})$, and it reads:
For the first potential [7]:

$$\begin{pmatrix}1 & 0 & 0 & 0 & 0\\ 0 & -\frac{\mathcal{J}-1}{\mathcal{J}} & \frac{\mathcal{J}+1}{\mathcal{J}}\frac{\sqrt{2\mathcal{J}-1}}{\sqrt{2\mathcal{J}+1}} & 0 & 0\\ 0 & \frac{\mathcal{J}+1}{\mathcal{J}}\frac{\sqrt{2\mathcal{J}-1}}{\sqrt{2\mathcal{J}+1}} & -\frac{1}{\mathcal{J}(\mathcal{J}+1)} & \frac{\mathcal{J}}{\mathcal{J}+1}\frac{\sqrt{2\mathcal{J}+3}}{\sqrt{2\mathcal{J}+1}} & 0\\ 0 & 0 & \frac{\mathcal{J}}{\mathcal{J}+1}\frac{\sqrt{2\mathcal{J}+3}}{\sqrt{2\mathcal{J}+1}} & -\frac{\mathcal{J}+2}{\mathcal{J}+1} & 0\\ 0 & 0 & 0 & 0 & 1\end{pmatrix} \tag{3}$$

For the second one [6]:

$$\begin{pmatrix}\frac{2(2-\mathcal{J})}{-3+6\mathcal{J}} & V_2^{--} & V_2^{-0} & 0 & 0\\ V_2^{--} & \frac{2(1-\mathcal{J}^2)}{3\mathcal{J}-6\mathcal{J}^2} & V_2^{+-} & 0 & 0\\ V_2^{-0} & V_2^{+-} & -\frac{2}{3\mathcal{J}(1+\mathcal{J})} & V_2^{00} & V_2^{+0}\\ 0 & 0 & V_2^{00} & \frac{2\mathcal{J}(2+\mathcal{J})}{9+15\mathcal{J}+6\mathcal{J}^2} & V_2^{-+}\\ 0 & 0 & V_2^{+0} & V_2^{-+} & -\frac{2(3+\mathcal{J})}{9+6\mathcal{J}}\end{pmatrix} \tag{4}$$

with,

$$\begin{aligned}V_2^{-0}&=\tfrac{\mathcal{J}+1}{\mathcal{J}(2\mathcal{J}-1)(2\mathcal{J}+1)}\\ V_2^{--}&=\tfrac{3\mathcal{J}-2}{2(2\mathcal{J}-1)\sqrt{\mathcal{J}(\mathcal{J}-1)}}\\ V_2^{+-}&=\tfrac{\mathcal{J}^2-\mathcal{J}-2}{3\mathcal{J}\sqrt{4\mathcal{J}^2-1}}\\ V_2^{00}&=\tfrac{\mathcal{J}(\mathcal{J}+3)}{3(\mathcal{J}+1)\sqrt{4\mathcal{J}(\mathcal{J}+2)+3}}\\ V_2^{-+}&=-\tfrac{\sqrt{2+\mathcal{J}}}{(3+2\mathcal{J})\sqrt{1-\mathcal{J}}}\\ V_2^{+0}&=\mathcal{J}\sqrt{\tfrac{(2+\mathcal{J})}{(1+\mathcal{J})(1+2\mathcal{J})(3+2\mathcal{J})}}\end{aligned}$$

The four dimensional box corresponds to the subspace spanned by $((P^{0-}_{1\mathcal{J}\mathcal{M}},P^{-0}_{1\mathcal{J}\mathcal{M}},P^{+0}_{1\mathcal{J}\mathcal{M}},P^{0+}_{1\mathcal{J}\mathcal{M}})$, and it reads:
For the first potential [7]:

$$\begin{pmatrix}\frac{1}{\mathcal{J}} & \frac{\sqrt{\mathcal{J}^2-1}}{\mathcal{J}} & 0 & 0\\ \frac{\sqrt{\mathcal{J}^2-1}}{\mathcal{J}} & -\frac{1}{\mathcal{J}} & 0 & 0\\ 0 & 0 & \frac{1}{\mathcal{J}+1} & \frac{\sqrt{(\mathcal{J}+2)\mathcal{J}}}{\mathcal{J}}\\ 0 & 0 & \frac{\sqrt{(\mathcal{J}+2)\mathcal{J}}}{\mathcal{J}} & -\frac{1}{\mathcal{J}+1}\end{pmatrix} \tag{5}$$

For the second one [6]:

$$\begin{pmatrix}\frac{2}{3\mathcal{J}} & V_2^{0--0} & V_2^{0-+0} & 0\\ V_2^{0--0} & -\frac{2}{3\mathcal{J}}+\frac{2}{1+2\mathcal{J}} & V_2^{-0+0} & \frac{\mathcal{J}\sqrt{1+\frac{1}{1+\mathcal{J}}}}{1+2\mathcal{J}}\\ V_2^{0-+0} & V_2^{-0+0} & -\frac{2(2+\mathcal{J})}{3+9\mathcal{J}+6\mathcal{J}^2} & V_2^{+00+}\\ 0 & \frac{\mathcal{J}\sqrt{1+\frac{1}{1+\mathcal{J}}}}{1+2\mathcal{J}} & V_2^{+00+} & -\frac{2}{3+3\mathcal{J}}\end{pmatrix} \tag{6}$$

with,

$$\begin{aligned}V_2^{0--0}&=\tfrac{\sqrt{\mathcal{J}^2-1}}{3\mathcal{J}}+\tfrac{\sqrt{\frac{\mathcal{J}-1}{\mathcal{J}}}(1+\mathcal{J})}{1+2\mathcal{J}}\\ V_2^{0-+0}&=\tfrac{(1+\mathcal{J})\sqrt{1-\frac{2}{1+2\mathcal{J}}}}{3\mathcal{J}}\\ V_2^{-0+0}&=\tfrac{\sqrt{\frac{\mathcal{J}}{1+\mathcal{J}}}-\sqrt{\frac{\mathcal{J}+1}{\mathcal{J}}}}{1+2\mathcal{J}}\\ V_2^{+00+}&=\tfrac{\sqrt{\mathcal{J}(2+\mathcal{J})(\mathcal{J}-1)}}{3(\mathcal{J}+1)(2\mathcal{J}+1)}\end{aligned}$$

If $J=1$, $P^{--}_{1\mathcal{J}\mathcal{M}}$ and $P^{0-}_{1\mathcal{J}\mathcal{M}}$ do not exist and the matrices are 7x7. If $J=0$, $P^{--}_{1\mathcal{J}\mathcal{M}},P^{+-}_{1\mathcal{J}\mathcal{M}},P^{00}_{1\mathcal{J}\mathcal{M}},P^{0-}_{1\mathcal{J}\mathcal{M}},P^{-0}_{1\mathcal{J}\mathcal{M}},P^{+0}_{1\mathcal{J}\mathcal{M}}$ do not exist and the system is reduced to 3x3 matrices for both potentials.

II. DEVELOPMENT

A. Identifying r_0

The form of $V_{hf}(r)$ and $V_{hf2}(r)$ is different at short and long distances.

Following [4], the potential can be rewritten in $(1/m)$ terms with spin-dependent and spin-independent parts. If the subdominant $(1/m)^2$ terms are neglected, the non-perturbative part is a series in powers of r: $V^{np}=V^{np(0)}+V^{np(1)}r^2+....$

In our case, at short distances:

$$V^s_{hf}=A+\mathcal{O}(r^2)\qquad V^s_{hf2}=Br^2+\mathcal{O}(r^4) \tag{7}$$

At long distances the energy spectrum of a static $Q\bar{Q}$ pair is well described by the QCD effective string theory. It has been obtained in [8]:

$$V^l_{hf}=-\frac{1}{6}\frac{gc_F\pi^2\Lambda'''}{m_Q\kappa r^3}\qquad V^l_{hf2}=\pm\frac{gc_F\Lambda'\pi^2}{2m_Q\sqrt{2\pi\kappa}}\frac{1}{r^2} \tag{8}$$

The parameters $g\Lambda'\sim\Lambda_{QCD}$ and $g\Lambda'''\sim\Lambda_{QCD}$ which have been calculated in [2].

$$g\Lambda'\sim -59MeV\quad ;\quad g\Lambda'''\sim\pm 230MeV \tag{9}$$

κ is the string tension and $c_F\approx 1$.

First, it is necessary to find the distance r_0 at witch the potential changes from short distances to long distances behaviour. To do so, we need to know the shape of $V_{\Sigma_u^-}$ and V_{Π_u} (the only hybrid interactions that we are

considering). They can be approximated by simple functions that have the correct behavior at short and long distances. The form we have taken is the same used in [2], were $V_{\Sigma_u^-}(r)$ is a Cornell-like potential, whereas for $V_{\Pi_u}(r)$ this type of potential does not fit the lattice data well at intermediate distances. Hence, a slightly more complicated form is taken:

$$V_{\Sigma_u^-}(r) = \frac{\sigma_s}{r} + \kappa_s r + E_s^{Q\bar{Q}} \tag{10}$$

$$V_{\Pi_u}(r) = \frac{\sigma_p}{r}\left(\frac{1+b_1 r + b_2 r^2}{1+a_1 r + a_2 r^2}\right) + \kappa_p r + E_p^{Q\bar{Q}} \tag{11}$$

Applying Taylor to Eq. (11), we find its behaviour at short and long distances:

$$V^s_{\Pi_u}(r) = \frac{\sigma_p}{r} + [\sigma_p(b_1 - a_1) + E_p^{Q\bar{Q}}] + [\sigma_p(a_1^2 - a_1 b_1 + b_2 - a_2) + \kappa_p]r + \mathcal{O}(r^2) \tag{12}$$

$$V^l_{\Pi_u}(r) = \sigma_p \frac{b_2}{a_2}\frac{1}{r} + E_p^{Q\bar{Q}} + \kappa_p r + \mathcal{O}(1/r^2) \tag{13}$$

r_0 is defined as the distance in where $V^s_{\Pi_u}(r)$ to $\mathcal{O}(r)$ and $V^l_{\Pi_u}(r)$ to $\mathcal{O}(1/r)$ are equal. Consequently,

$$r_0 = \frac{\sigma_p(b_1 - a_1) \pm \sqrt{[\sigma_p(b_1 - a_1)]^2 + 4\kappa_p\sigma_p}}{2\kappa_p} \tag{14}$$

The coefficients are required to satisfy the following system of equations:

$$\sigma_p(b_1 - a_1) + (E_p^{Q\bar{Q}} - E_s^{Q\bar{Q}}) = 0 \tag{15}$$

$$a_1^2 - a_1 b_b + b_2 - a_2 + \frac{\kappa_p}{\sigma_p} = 0 \tag{16}$$

$$\sigma_p b_2 = \frac{11\pi}{12} \tag{17}$$

Eq. (15) results out of the coincidence of $V^s_{\Pi_u}(r)$, at short distances, with $V_{\Sigma_u^-}(r)$, which also implies $\sigma_s = \sigma_p$. At short distances, the correction of the constant term of V_{Π_u} is $\mathcal{O}(r^2)$, therefore, $\mathcal{O}(r) = 0$ (16). In (17) we are matching the $\mathcal{O}(1/r)$ term of the potential at long distances to its theoretical prediction in string theory.

From [2] we obtain:

$$\begin{gathered}\sigma_s = \sigma_p = \sigma = 0.061 \\ \kappa_s = \kappa_p = \kappa = 0.187 GeV^2 r \\ E_s^{c\bar{c}} = 0.559 GeV, \qquad E_s^{b\bar{b}} = 0.573 GeV\end{gathered} \tag{18}$$

Fitting potential (11) to lattice data with coefficients (18), we found:

$$\begin{gathered}a_1 = 0 GeV, \qquad a_2 = -0.0662 GeV^2 \\ b_1 = 11.9 GeV^2, \qquad b_2 = -3.131913 GeV^2 \\ E_p^{c\bar{c}} = -0.1666899 GeV, \qquad E_p^{b\bar{b}} = -0.1529 GeV\end{gathered} \tag{19}$$

And

$$r_0 = 3.964 GeV^{-1} \tag{20}$$

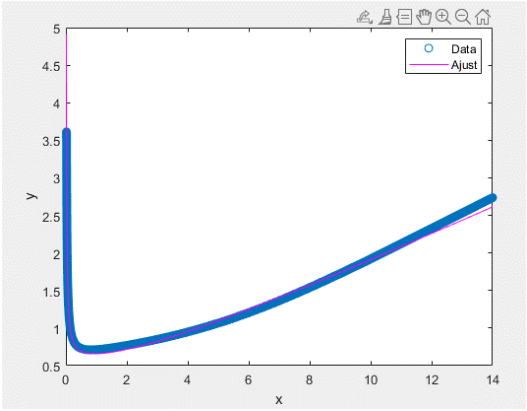

FIG. 2: Fitting of $V_{\Pi_u}(r)$ with lattice data in MATLAB with the coefficients of (18) and (19). The magenta line is our fit, and the blue one is the fit done in [2] of the lattice data. Axis: $x = r(GeV^{-1})$ and $y = V(GeV)$

B. Interpolation of the potentials

To precisely calculate the spectrum including hyperfine splitting of charmonium, we need to find an interpolation of $V_{hf}(r)$ and $V_{hf2}(r)$ that could work for all the range. We also will be able to calculate the spectrum of bottomonium. But, as we do not have lattice data to check it, we would only be doing predictions and we can not find the accuracy of our interpolations with it. Hence, the fitting of the interpolations will be done only with charmonium lattice data.

We need to find smooth functions that show proper behaviour at short and long distances. Having (7) and (8) in mind and knowing that the change of behaviour is done approximately at r_0 (20), we model the hyperfine potential making explicit the signs of $g\Lambda'''$ and $g\Lambda'$ as Eq. (21).

$$V_{hf} = \frac{A \pm \left(\frac{r}{r_0}\right)^2 \frac{1}{r_1}}{1 + \left(\frac{r}{r_0}\right)^5} \qquad V_{hf2} = \frac{Br^2 \pm \left(\frac{r}{r_0}\right)^4 \frac{1}{r_2}}{1 + \left(\frac{r}{r_0}\right)^6} \tag{21}$$

$$\frac{1}{r_1} = \left(\frac{|g\Lambda'''|c_F\pi^2}{6m_Q\kappa}\right)\frac{1}{r_0^3} \qquad \frac{1}{r_2} = \left(\frac{|g\Lambda'|c_F\pi^2}{2m_Q\sqrt{2\pi\kappa}}\right)\frac{1}{r_0^2}$$

C. Spectrum

To calculate the best fits for A and B, we run a program and check different values while searching for the lowest χ^2/dof comparing the spectrum obtained with lattice data from [3]. We repeat this procedure with each sign combination of (21) to find the most suitable signs and values.

The formula used to calculate χ^2 is (22). Dof are the degrees of freedom of each calculation (number of values

calculated − number of unknown factors).

$$\chi^2 = \sum_i \frac{[(\text{our value})_i - (\text{lattice data})_i]^2}{(\text{uncertainty}_i)^2} \qquad (22)$$

The lattice data used is the masses for charmonium spectrum computed by [3]. We only utilize the states identified as hybrid mesons. Red states are the group formed by the lightest multiplet; and blue states are the first-excited supermultiplet. (Table I)
The Hadronic Spectrum Collaboration has calculated the charmonium spectrum including hybrid states, where smaller quark masses are taken for up and down. Therefore, the order of the lowest lying hybrid multiplets in [3] is the same as ours, from lighter to heavier: $1(s/d)_1$, $1p_1$, $1(p/f)_2$ and $1p_0$; but, their numbers are larger than our spin averages calculated with (11) and (10). This incompatibility can be solved subtracting respectively in each multiplet: 381 MeV, 326 MeV, 392 MeV and 151 MeV.

Our aim is to find if taking into account the long distance behaviour of the hyperfine potential improves the results, to do so we compute the spectrum with and without it.

First, we use as V_{hf} and V_{hf2} their short distances shape (7). We calculated the spectrum with $V_{hf} = A$ and $V_{hf2} = 0$; $V_{hf} = 0$ and $V_{hf2} = Br^2$; $V_{hf} = A$ and $V_{hf2} = Br^2$. In the last combination we utilize, to find the constants, two procedures: fitting only with the red states and fitting with the red and blue states. With the last method, which should be the most accurate, we obtain the spectrum shown in Table II and the following fits: $A = 0.0699GeV$, $B = 0.0008GeV^3$ with $\chi^2/dof = 1.1927$.

Then, the calculus are repeated using the interpolations made for V_{hf} and V_{hf2} (21). All the possible signs combination are tested. First, only with V_{hf}, then only with V_{hf2}, and, lastly, with both interpolations and fitting with red states and then red and blue states. We obtain that the sign combination that gives the best (lowest) χ^2/dof is (23). And the best fits are $A = 0.1175GeV$, $B = 0.0057GeV^3$ with $\chi^2/dof = 0.67583$ and the spectrum of Table III.

The main difference between our calculus and [4] reside in this spectrum where we are taking into account the long distance behaviour of the potentials V_{hf} and V_{hf2} correctly.

$$V_{hf} = \frac{A - \left(\frac{r}{r_0}\right)^2 \frac{1}{r_1}}{1 + \left(\frac{r}{r_0}\right)^5} \qquad V_{hf2} = \frac{Br^2 - \left(\frac{r}{r_0}\right)^4 \frac{1}{r_2}}{1 + \left(\frac{r}{r_0}\right)^6} \qquad (23)$$

$$\frac{1}{r_1} = \left(\frac{|g\Lambda'''|c_F\pi^2}{6m_Q\kappa}\right)\frac{1}{r_0^3} \qquad \frac{1}{r_2} = \left(\frac{|g\Lambda'|c_F\pi^2}{2m_Q\sqrt{2\pi\kappa}}\right)\frac{1}{r_0^2}$$

1. *Bottomonium*

There is no lattice data of hyperfine spectrum of bottomonium hence if we calculate it, it will only be a prediction.

Knowing the best fits for the constants A and B for charmonium, we can now calculate the spectrum for bottomonium. The constants in this case are $A' = Am_c/m_b = 0.035398GeV$ and $B' = Bm_c/m_b = 0.001717GeV^3$ ($m_c = 1.4702GeV$ and $m_b = 4.8802GeV$). We obtain the spectrum of Table IV.

	State	$\mathcal{J}^{PC}$	**M (GeV)**	**Uncertainty (GeV)**
Red	$(s/d)_1$	1^{--}	4.030	0.018
	$(s/d)_1$	0^{-+}	3.898	0.019
	$(s/d)_1$	1^{-+}	3.929	0.024
	$(s/d)_1$	2^{-+}	4.075	0.022
Blue	p_1	0^{+-}	4.111	0.028
	p_1	2^{+-}	4.176	0.019
	$(p/f)_2$	2^{+-}	4.239	0.027
	p_0	0^{-+}	4.440	0.047
	p_1	1^{+-}	4.112	0.024
	$(p/f)_2$	1^{+-}	4.179	0.028
	p_0	1^{+-}	4.514	0.054
	p_1	1^{++}	4.144	0.026
	$(p/f)_2$	2^{++}	4.231	0.033
	$(p/f)_2$	3^{+-}	4.252	0.035

TABLE I: Charmonium. Upper table: shows the mass of the red states used as lattice data. Lower table: shows the mass of the blue states. The values are the ones in [3] corrected to equal the spin average of [2].

	State	$\mathcal{J}^{PC}$	**M (GeV)**
Red	$(s/d)_1$	1^{--}	4.011
	$(s/d)_1$	0^{-+}	3.920
	$(s/d)_1$	1^{-+}	3.965
	$(s/d)_1$	2^{-+}	4.054
Blue	p_1	0^{+-}	4.091
	p_1	2^{+-}	4.144
	$(p/f)_2$	2^{+-}	4.238
	p_0	0^{-+}	4.486
	p_1	1^{+-}	4.082
	$(p/f)_2$	1^{+-}	4.198
	p_0	1^{+-}	4.442
	p_1	1^{++}	4.145
	$(p/f)_2$	2^{++}	4.232
	$(p/f)_2$	3^{+-}	4.169

$\chi^2/dof = 1.1927$

TABLE II: Charmonium. First table: shows the mass of the red states. Second table: shows the mass of the blue states. Both calculated with (7) and $A = 0.0699GeV$, $B = 0.0008GeV^3$. Third table: χ^2/dof obtained ($\chi^2 = 14.3124$ and $dof = 12$) fitted with red and blue states.

	State	$\mathcal{J}^{PC}$	M (GeV)
Red	$(s/d)_1$	1^{--}	4.011
	$(s/d)_1$	0^{-+}	3.899
	$(s/d)_1$	1^{-+}	3.956
	$(s/d)_1$	2^{-+}	4.061
Blue	p_1	0^{+-}	4.095
	p_1	2^{+-}	4.148
	$(p/f)_2$	2^{+-}	4.234
	p_0	0^{-+}	4.486
	p_1	1^{+-}	4.098
	$(p/f)_2$	1^{+-}	4.196
	p_0	1^{+-}	4.462
	p_1	1^{++}	4.145
	$(p/f)_2$	2^{++}	4.232
	$(p/f)_2$	3^{+-}	4.260

$\chi^2/dof = 0.67583$

TABLE III: Charmonium. First table: shows the mass of the red states. Second table: shows the mass of the blue states. Both calculated with (23) and $A = 0.1175GeV$, $B = 0.0057GeV^3$. Third table: χ^2/dof obtained ($\chi^2 = 8.1100$ and $dof = 12$) fitted with red and blue states.

III. CONCLUSIONS

We have accomplished the calculus of hyperfine spectrum of charmonium with a considerably low χ^2/dof in relation to the results of [3]. Comparing results of Table II and Table III, it is clear that taking into account the large distances behaviour of the hyperfine potentials significantly improves the results. With the potentials found (23) it has been possible to calculate the bottomonium spectrum in Table IV including the hyperfine splittings.

	State	$\mathcal{J}^{PC}$	M (GeV)
Red	$(s/d)_1$	1^{--}	10.690
	$(s/d)_1$	0^{-+}	10.679
	$(s/d)_1$	1^{-+}	10.684
	$(s/d)_1$	2^{-+}	10.696
Blue	p_1	0^{+-}	10.755
	p_1	2^{+-}	10.764
	$(p/f)_2$	2^{+-}	10.817
	p_0	0^{-+}	11.300
	p_1	1^{+-}	10.760
	$(p/f)_2$	1^{+-}	10.819
	p_0	1^{+-}	11.012
	p_1	1^{++}	10.761
	$(p/f)_2$	2^{++}	10.819
	$(p/f)_2$	3^{+-}	10.823

TABLE IV: Bottomonium. Upper table: shows the mass of the red states. Lower table: shows the mass of the blue states. Both calculated with the potentials (23) and the constants $A' = 0.035398GeV$ and $B' = 0.001717GeV^3$

Acknowledgments

All this work could have never be done without my advisor Joan Soto who gave me the opportunity to do an internship with him and then continue the work within this TFG while explaining me all I needed. Of course, I am grateful for my parents who supported me and made possible my studies in Universitat de Barcelona. Also, recall all the professors who taught me everything.

[1] J. Soto, "Heavy Quarkonium Hybrids," Nucl. Part. Phys. Proc. **294-296** (2018), 87-94 doi:10.1016/j.nuclphysbps.2018.03.020 [arXiv:1709.08038 [hep-ph]].

[2] R. Oncala and J. Soto, "Heavy Quarkonium Hybrids: Spectrum, Decay and Mixing," Phys. Rev. D **96** (2017) no.1, 014004 doi:10.1103/PhysRevD.96.014004 [arXiv:1702.03900 [hep-ph]].

[3] G. K. C. Cheung *et al.* [Hadron Spectrum], "Excited and exotic charmonium, D_s and D meson spectra for two light quark masses from lattice QCD," JHEP **12** (2016), 089 doi:10.1007/JHEP12(2016)089 [arXiv:1610.01073 [hep-lat]].

[4] N. Brambilla, W. K. Lai, J. Segovia, J. Tarrús Castellà and A. Vairo, "Spin structure of heavy-quark hybrids," Phys. Rev. D **99** (2019) no.1, 014017 [erratum: Phys. Rev. D **101** (2020) no.9, 099902] doi:10.1103/PhysRevD.99.014017 [arXiv:1805.07713 [hep-ph]].

[5] K. J. Juge, J. Kuti and C. Morningstar, "Fine structure of the QCD string spectrum," Phys. Rev. Lett. **90** (2003), 161601 doi:10.1103/PhysRevLett.90.161601 [arXiv:hep-lat/0207004 [hep-lat]].

[6] P. Molina Grífols, "Spin-dependent Effects on the Hyperfine Structure in Heavy Hybrid Mesons," Bachelor Thesis, Universitat de Barcelona (February 2021)

[7] P. Solé Campreciós, "Heavy Hybrids Mesons in NRQCD: Fine and Hyperfine Structure," Bachelor Thesis, Universitat de Barcelona (June 2017)

[8] J. Castillo Uviña, "Spin Dependent Potential of the Heavy Hybird Mesons," Bachelor Thesis, Universitat de Barcelona (January 2020)